Ukrainian Journal of Physical Optics
ISSUE 1
2025

ORGANIC LIGHT-EMITTING DEVICES WITH QUANTUM WELL STRUCTURES USING CARBAZOLE DERIVATIVE 4CZTPN-PH AS AN EMITTING MATERIAL

L. DEVA[1], P. STAKHIRA[1]*, V. FITIO[1], S. DEBATA[2], P. DEV[2], N. KARAUSH-KARMAZIN[3], N. KUZYK[1], I. YAREMCHUK[1], D. VOLYNIUK[4]

[1] Department of Electronic Engineering, Lviv Polytechnic National University, 12 Bandera Street, 79013 Lviv, Ukraine
[2] Department of Physics and Astronomy, Howard University, Washington, D.C. 20059, USA
[3] Department of Chemistry and Nanomaterials Science, Bohdan Khmelnytsky National University of Cherkasy, 81 Shevchenko Boulevard, 18031 Cherkasy, Ukraine
[4] Department of Polymer Chemistry and Technology, Kaunas University of Technology, 59 Baršausko, 51423 Kaunas, Lithuania
*Corresponding author: pavlo.y.stakhira@lpnu.ua

Received: 07.10.2024

Abstract. Herein, we investigate the electroluminescent properties of organic light-emitting diodes (OLEDs) based on a carbazole derivative 2,3,5,6-tetrakis(3,6-diphenyl-9H-carbazol-9-yl)-1,4-benzenedicarbonitrile (4CzTPN-Ph) with red emission. Two types of OLEDs were fabricated using this emitter: the first employed a host-guest system, while the second utilized a light-emitting structure with a triple cascade of quantum wells. In the second OLED, an ultrathin 4CzTPN-Ph emitter layer with 5 nm thickness was placed between the layers of 3,3′-di(9H-carbazol-9-yl)-1,1′-biphenyl (mCBP) and diphenyl[4-(triphenylsilyl)phenyl]phosphine oxide (TSPO1) forming the first well, and between the same type of TSPO1 layers in the second and third quantum wells. This configuration made it possible to create optimal energy barriers at the interfaces to scatter charge carriers and excitons within each well efficiently. This configuration also contributed to expanding the carrier recombination zone and reducing the exciton quenching probability. Discrete energy levels for electrons and holes in the quantum wells were calculated by solving the stationary Schrödinger equation in the frequency domain. The calculations showed the localization of electrons and holes in the corresponding quantum wells. A comparative analysis of the efficiency of OLED devices (brightness, power efficiency, and current efficiency) showed that in the first type of OLED, efficient energy transfer to the 4CzTPN-Ph emitter was achieved due to the relatively broad spectral overlap between the emission spectrum of the host component (mCBP) and the absorption spectrum of the 4CzTPN-Ph emitter. As a result, the OLED with the host-guest system achieved an external quantum efficiency of 2% at a maximum brightness of more than 1000 cd/m^2. While the second type of device demonstrated slightly lower efficiency, the advantage of the quantum wells cascade structure lies in its narrow quantum wells (5 nm), which result in a characteristic narrowing of the electroluminescence spectra. This produces spectrally purer red emission with International Commission on Illumination (CIE) coordinates of (0.58, 0.33), compared to the broader spectrum of the doped OLED with CIE coordinates of (0.51, 0.38). This approach effectively solves the problem of red-to-blue spectrum shift inherent in OLED with a host-guest system.

Keywords: OLED, quantum well, exciton, heterostructure, host-guest system
UDC: 535.37
DOI: 10.3116/16091833/Ukr.J.Phys.Opt.2025.01009

1. Introduction

The competitiveness of modern full-color displays and solid-state lighting sources has significantly increased due to the advancements in the quality of red radiation, one of the three basic colors (red, green, and blue) [1]. The peak wavelength value in the electroluminescent emission (EL) spectrum of red organic light-emitting diodes (OLEDs)

must be outside 600 nm, and the International Commission on Illumination (CIE) coordinates of such organic light emitting devices shall correspond to $x \geq 0.60$ and $y \leq 0.40$ [2]. The red-emitting organic semiconductors in the OLED emitter layer typically have a narrow band gap, which is the energy difference between the highest occupied π-orbital (HOMO) and the lowest unoccupied molecular orbital (LUMO). This narrow gap results from the rigid planar coupling in the molecular systems of red emitters [3]. Usually, for emitters, the probability of non-radiative recombination of excited states increases as the energy gap decreases (the energy gap law), leading to low radiation efficiency [4]. Recent developments in the field of red organic LEDs have mainly focused on materials with a molecular structure based on the donor (D)-acceptor (A) type, which is characterized by the mechanism of thermally activated delayed fluorescence (TADF), with the theoretical internal quantum efficiency reaching up to 100% [5]. In such D-A emitters, the intramolecular transfer mechanism makes it possible to reduce the energy of singlet-triplet splitting to such values that the thermal energy at room temperature is sufficient to activate the reverse intersystem crossing (RISC), thereby contributing to the transformation of triplet excitons in radiative recombination. However, the efficiency of red and infrared OLEDs [6] remains limited due to triplet quenching, which occurs due to triplet-triplet annihilation [7–9]. From the point of view of OLED design, triplet quenching can be reduced by using a host-guest doping system to fabricate red and infrared OLEDs based on TADF emitters. Nevertheless, such an approach is a complex technological problem with often non-reproducible results, which limits the serial production of such devices [10]. In addition, during red OLED fabrication, an EL shift to the blue region of the spectrum relative to the photoluminescence spectrum of the emitter film is often observed [11,12]. This shift is attributed to the choice of matrix material with a significant dipole moment and the concentration of the emitter impurity in the OLED structure. An effective solution to this problem, which does not require the procedure of doping the emitter into the matrix material, is to use the OLED emitter as the integral component of a multilayer heterostructure, in which one thin active layer (less than 10 nm, approximately the de Broglie wavelength of the charge carriers) is placed between two wide bandgap semiconductor layers of nanoscale thickness [13]. With such a configuration, it is energetically beneficial for electrons and holes in the potential well to localize on the emitter with minimally small effective distances between them. As a result, the bond energy of the electron-hole pair (excitons) increases. Thus, light-emitting devices based on quantum wells (QWs) are realized due to quantum limitations [14], which provide tuning of electroluminescent characteristics. Taking into account the above reports, in this paper, we investigate in detail the localization of electrons and holes in quantum wells at certain discrete energy levels, the corresponding wave functions, and the electroluminescence properties of OLEDs with host-guest and multiple quantum well (MQW) structures using 2,3,5,6-tetrakis(3,6-diphenylcarbazol-9-yl)-1,4-dicyanobenzene (4CzTPN-Ph) as a red TADF emitter [15, 16].

2. Computational details

We employed plane wave density functional theory to compute the effective mass of the 4CzTPN-Ph crystal system. The calculations were performed using the Quantum Espresso package [17], where we used the generalized gradient approximation (GGA) with the Perdew–Burke–Ernzerhof (PBE) functional to account for exchange-correlation effects [18].

As the van der Waals interactions play an important role in such systems, we included the Grimme-D3 correction scheme [19] to account for the dispersion interactions. We used the plane wave energy cutoffs of 50 Ry (680.29 eV) and 350 Ry (4761.99 eV) to expand the wavefunctions and charge densities. The crystal structure was consistent with that of the experimental observation. A Γ-centered k-point mesh grid of 3×4×2 was used to sample the Brillouin zone for self-consistent calculations.

3. Results and discussion

3.1. OLED fabrication

To achieve spectrally pure red OLEDs with an emission wavelength of around 620 nm, a quantum well-based OLED using a 4CzTPN-Ph emitter (Fig. 1a) with an ultra-thin light-emitting layer (EML) was fabricated, along with a reference OLED. The reference OLED is a device in the architecture of which 4CzTPN-Ph is a dopant in a wide-bandgap organic semiconductor matrix (Fig. 1b).

The reference OLED, without quantum wells (Fig. 1b, Device A) with the structure: ITO/CuI (5 nm)/TAPC (40 nm)/mCBP : 4CzTPN-Ph (40 nm)/TSPO1 (10 nm)/TPBi (40 nm)/Ca (2 nm)/Al was fabricated by thermal deposition in a vacuum chamber (10^{-5} Torr) on a glass substrate coated with a transparent conductive layer of Indium Tin Oxide (ITO). The device structure was formed through a stepwise deposition of active layers: Copper Iodide (CuI) as the hole-injection layer [20], 1,1-Bis[(di-4-tolylamino)phenyl]cyclohexane (TAPC) as the hole-transport layer [21], and diphenyl[4-(triphenylsilyl)phenyl]phosphine oxide (TSPO1) as the hole-blocking layer [22]. 2,2',2''-(1, 3,5-Benzinetriyl)-tris(1-phenyl-1-H-benzimidazole) (TPBi) [12] was selected for ensuring good transport of electrons. The red ambipolar emitter 4CzTPN-Ph was doped into the matrix 3,3′-Di(9H-carbazol-9-yl)-1,1′-biphenyl (mCBP) [23] by the method of controlled co-deposition from two crucibles (in a ratio of 50:50). The Ca:Al film served as the cathode.

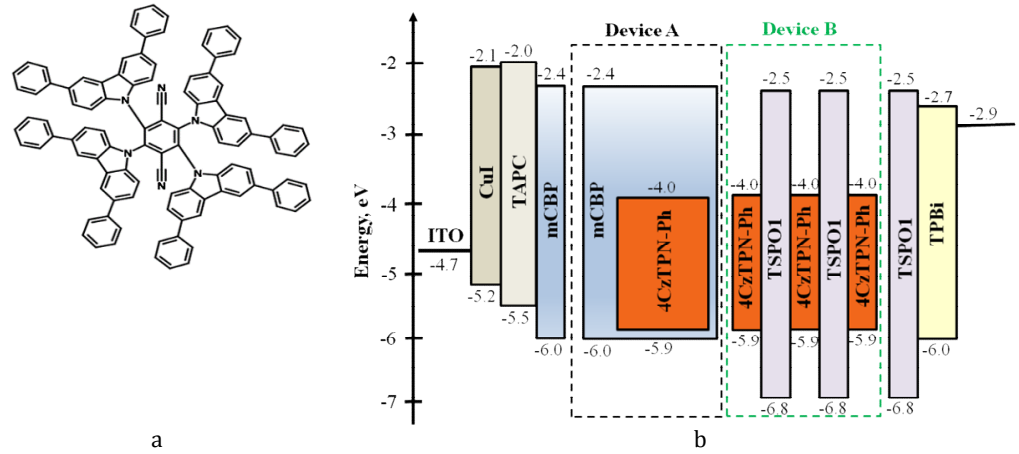

a b

Fig. 1. (a) Chemical structure of 2,3,5,6-tetrakis(3,6-diphenyl-9H-carbazol-9-yl)-1,4-benzenedicarbonitrile (4CzTPN-Ph). (b) Energy level diagram of doped (reference) OLED (Device A) and QW-OLED with a structure of quantum wells (Device B).

The key difference in the structure of the light-emitting device (Fig. 1b, Device A) compared to the quantum wells structure (Fig. 1b, Device B) lies in the absence of a host-guest system and the inclusion of a cascade of three QWs (n=3). In Device B, an ultrathin film of 4CzTPN- Ph was placed between the layers of mCBP and TSPO1, forming the first QW, and between identical TSPO1 layers for the second and third QWs. The complete structure is as follows: ITO/CuI

(5 nm)/TAPC (40 nm)/mCBP (15 nm)/ 4CzTPN-Ph (5 nm)/ TSPO1 (5 nm)/ 4CzTPN-Ph (5 nm)/ TSPO1 (5 nm)/ 4CzTPN- Ph (5 nm)/TSPO1 (10 nm)/TPBi (40 nm)/Ca (2 nm)/Al.

In this work, all materials (ITO, Ca, Al, CuI, TAPC, mCBP, 4CzTPN-Ph, TSPO1, TPBi) were obtained commercially and used directly without further purification. All devices were manufactured without additional sealing and tested in an ambient atmosphere at room temperature.

The choice of mCBP as the matrix material is due to the position of the first triplet energy level (T_1 = 2.91 eV) [24], which is higher than the triplet state of the 4CzTPN-Ph emitter (T_1 = 2.21 eV) [16], ensuring the avoidance of energy leakage through the triplet levels of the matrix [25]. Furthermore, due to a low dipole moment of the mCBP host component (μ_D=2.5 [26]), the electroluminescence spectrum of Device A was shifted to the short-wavelength region with a maximum of 612 nm relative to the photoluminescence spectrum of the 4CzTPN-Ph thin film with a maximum near 624 nm (Fig. 2a, insert).

The EL performances of the fabricated Devices A and B are presented in Fig. 2 and summarized in Table 1. Device A shows a rather low turn-on voltage and stable brightness characteristics in a wide current density range, implying that the structure based on the host-guest system with the 4CzTPN-Ph emitter is stable to the applied voltage. The EQE roll-off for Device A is negligible, probably due to balanced charge trapping in the emissive layer.

Table 1. The electrical characteristics of red reference OLED (Device A) and QW-OLED with a structure of quantum wells (Device B).

Device	Turn-on voltage, V	Maximum luminance, cd/m²	CE_{max}[a], cd/A	PE_{max}[b], lm/W	EQE_{max}[c], %	CIE[d], x, y
A	3.7	1012.15	2.60	0.85	1.90	(0.51, 0.38)
B	6.0	419.75	1.82	0.49	1.29	(0.58, 0.33)

[a] CE_{max}: Maximum current efficiency. [b] PE_{max}: Maximum power efficiency. [c] EQE_{max}: Maximum external quantum efficiency. [d] $CIE_{x,y}$: CIE coordinates at 10 mA cm^{-2}.

It is known that in devices with QW structure, when the width of the well exceeds 2 nm, the possibility of excimer formation in the potential well layer (PWL) emitter increases, especially for narrow-band TADF materials [27]. Therefore, the probability of a red shift increases and may ultimately exceed the probability of a shift to the blue region of the EL spectrum. Considering these analytical considerations, the PWL width for the OLED structure with triple quantum wells (Device B) was set at 5 nm in this work.

From the energy level diagram of Device B (Fig. 1b), it can be observed that the energy barriers of the electron interface between the potential barrier layer (PBL) and PWL are 1.5 eV, causing charges to localize in PWL, followed by exciton radiative recombination. The energy positions of the first triplet levels for mCBP [24] and TSPO1 [22] are 2.91 eV and 3.36 eV, respectively, they are higher than T_1 = 2.21 eV of the 4CzTPN-Ph-based emitter [16], ensuring triplet exciton retention in the emission layer. The EL spectra of Device B show a peak emission at 618 nm (Fig. 2c, inset), with a 7 nm red shift and emission spectral narrowing compared to Device A and the emitter's photoluminescence spectrum (Fig. 2a, inset, and Fig. 2c, inset). This is a significant advantage for QW devices, as a narrow EL spectrum and pure red CIE coordinates are prioritized for RGB applications. The color coordinates (x, y) according to the CIE 1931 standard for devices A and B are (0.51; 0.38) and (0.58; 0.33), respectively (Fig. 3).

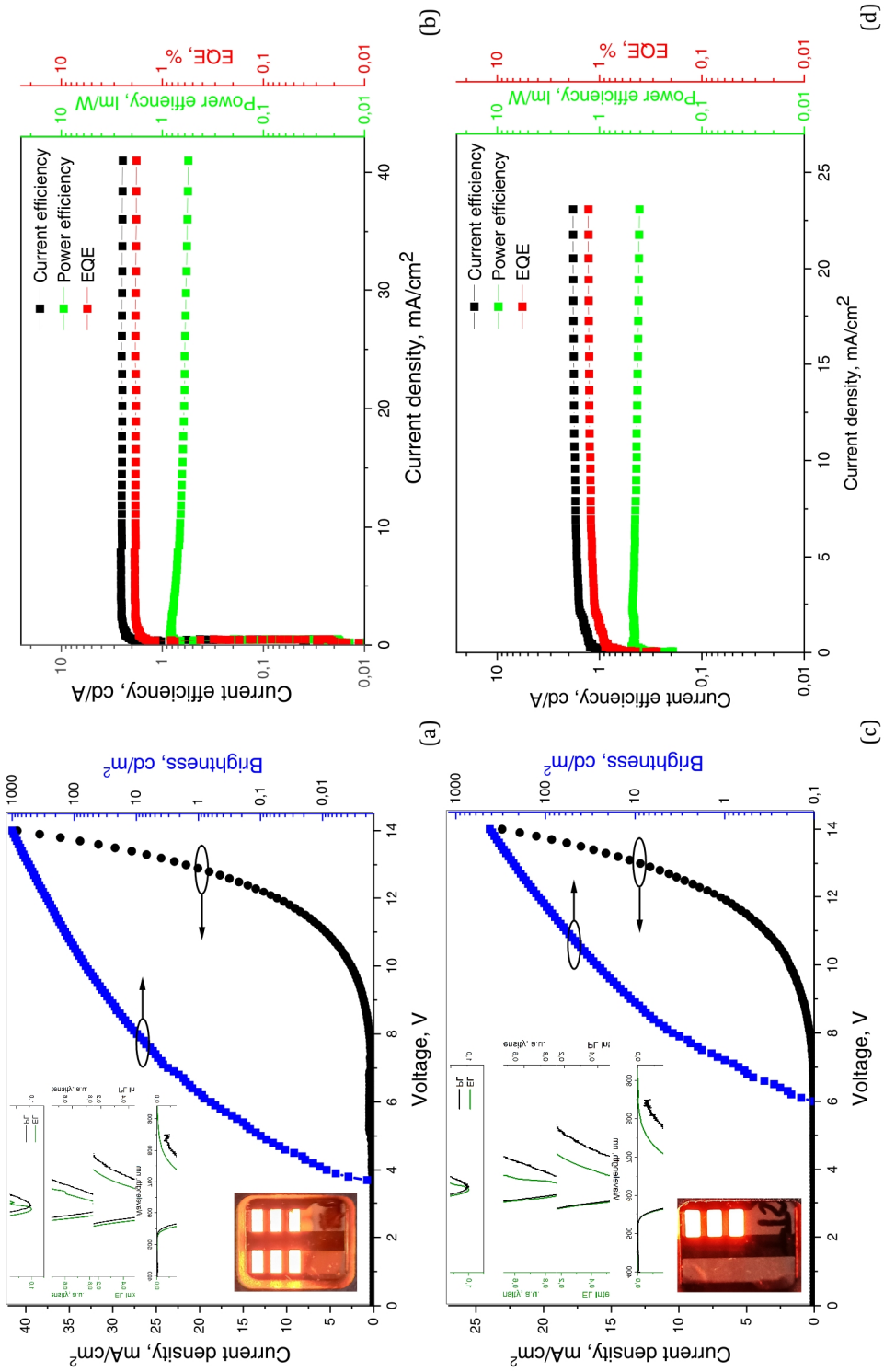

Fig. 2. Current density-voltage and brightness-voltage characteristics of Devices A (a) and B (c). (Inserts: The EL spectrum (at 14 V) and the thin film PL spectrum of EML layers and the images of the fabricated Devices A and B, respectively). Current efficiency, power efficiency, and external quantum efficiency (EQE) dependencies on the current density of Devices A (b) and B (d).

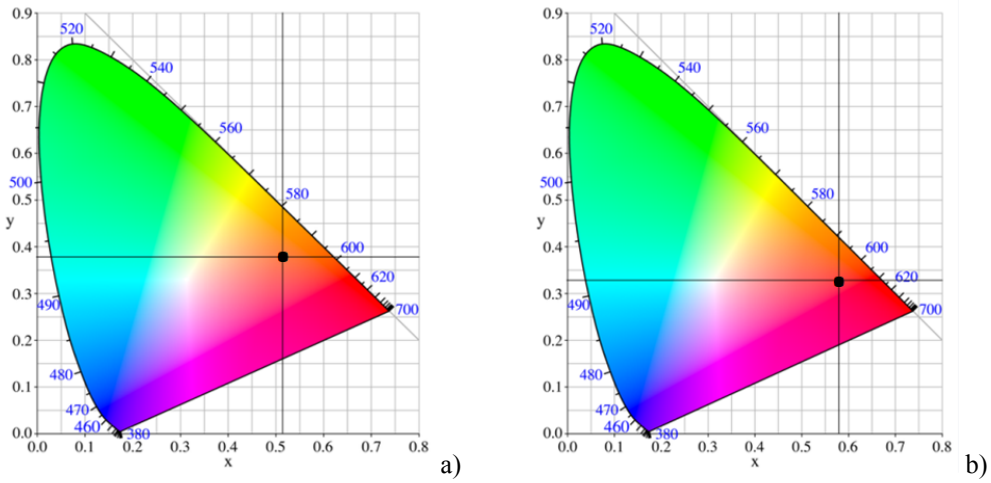

Fig. 3. CIE 1931 chromaticity diagram of Devices A (a) and B (b). The black points correspond to the color coordinates of the devices.

It should be noted that the slightly higher turn-on voltage and lower maximum EQE of Device B compared to Device A (Table 1) are probably due to deep traps in the PWL/EML interface. These traps require electrons to overcome the PWL energy barrier at higher applied voltage [28]. Overall, Device B is found to have lower current consumption (Fig. 2b and Fig. 2d).

3.2. Band structure and effective mass of charge carriers

The 4CzTPN-Ph crystal adopts a monoclinic structure (Fig. 4a). In Fig. 4b, we plot the Brillouin zone for the crystal, showing the high symmetry points. The electronic band structure shown in Fig. 4c reveals an indirect bandgap of 1.22 eV, with the valence band maximum (VBM) located at the Γ-point and the conduction band minimum (CBM) between Γ and Y-points. The direct bandgap at the Γ-point is found to be 1.26 eV.

To understand the transport properties of the 4CzTPN-Ph crystal, it is important to determine the effective masses for the electrons (m_e^*) and hole (m_h^*). We calculated the effective masses of charge carriers using the following formula:

$$m^* = \frac{\hbar^2}{\partial^2 E / \partial k^2}, \tag{1}$$

where m^* is the effective mass, $\hbar$ is the reduced Planck's constant, and $\partial^2 E / \partial k^2$ represents the curvature of the band structure. Along with the parabolic fits, Figs. 4d and 4e show our density functional theory (DFT) results for the band structure of the 4CzTPN-Ph crystal along the Γ-Z direction close to the maximum and the minimum in the valence and conduction bands, respectively. These plots show that close to the maximum and the minimum, the parabolic fit is a good approximation. By fitting the parabolic band around the minimum in the conduction band in the Γ-Z direction, we obtain an electron effective mass, m_e^*, of $11.30 m_o$ where m_o is the free electron mass.

In contrast, the hole effective mass m_h^* value along the same direction was calculated to be -$2.26 m_o$. We find that the effective mass for electrons is higher than that for the hole, which is a consequence of the lower curvature of the CBM compared to VBM. This suggests that the molecular structure of 4CzTPN-Ph, consisting of multiple carbazole units, is preferable for higher hole mobility than electron mobility, making it well-suited for OLED applications [15, 16, 29–31].

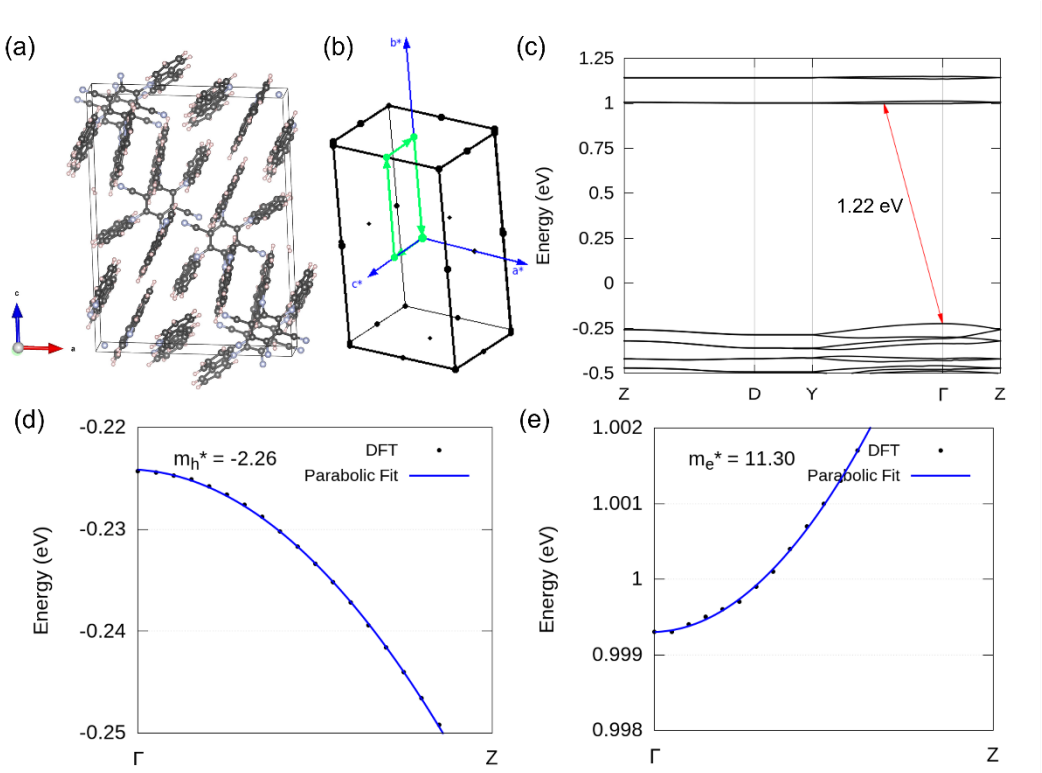

Fig. 4. (a) the crystal structure of 4CzTPN-Ph, (b) the corresponding bulk Brillouin zone showing the high-symmetry points, and (c) the electronic band structure of 4CzTPN-Ph crystal. (d) and (e) show parabolic fitting for the VBM and the CBM along the Γ-Z direction, respectively. The parabolic curve fitting is used to estimate the effective hole and electron masses.

3.3. Calculation of discrete levels of electrons and holes in quantum wells

The one-dimensional stationary Schrödinger equation was used to calculate the discrete levels of electrons and holes in quantum wells (Device B):

$$-\frac{\hbar^2}{2m}\frac{d^2\psi(x)}{dx^2}+U_0(x)\psi(x)=E_0\psi(x), \tag{2}$$

where $\psi(x)$ is a wave function. The parameter m is the mass of a quantum particle, U_0 is the potential energy representing the environment in which the quantum particle exists, and E_0 is the energy of the quantum particle.

This equation was modified by multiplying the right and left sides of the equation by $\frac{2m}{\hbar^2}$. The dimensionless Eq. (2) can be presented as:

$$-\frac{d^2\psi(x)}{dx^2}+U(x\psi(x))=E\psi(x), \tag{3}$$

where $U(x)=\frac{2m}{\hbar^2}U_0(x), E=\frac{2m}{\hbar^2}E_0$.

The solution of the stationary Schrödinger equation $\psi(x)$, corresponds to discrete energy levels, and their primary derivatives tend to zero at $x\to\pm\infty$. Therefore, the Fourier transform for these functions and their primary and secondary derivatives exists, which are equal [32]:

$$\psi(u) = \int_{-\infty}^{\infty} \psi(x) \exp(-i2\pi ux) dx , \tag{4}$$

$$i2\pi u\psi(u) = \int_{-\infty}^{\infty} \frac{d\psi(x)}{dx} \exp(-i2\pi ux) dx , \tag{5}$$

$$-(2\pi u)^2 \psi(u) = \int_{-\infty}^{\infty} \frac{d^2\psi(x)}{dx^2} \exp(-i2\pi ux) dx. \tag{6}$$

If there is a Fourier transform for two functions $g(x)$ and $h(x)$, i.e. $F\{g(x)\} = G(u)$, $F\{h(x)\} = H(u)$, the following relation is also valid [33]:

$$F\{g(x)h(x)\} = \int_{-\infty}^{\infty} G(u-v)H(v) dv , \tag{7}$$

where $F\{...\}$ denotes the Fourier transform of an integrated function; u and v are the coordinates in the frequency domain. Expression (6) describes the content of the convolution theorem.

As a result of the Fourier transformation of the right and left parts of Eq. (2) using (3), (6) and (7), the following equation was obtained:

$$4\pi^2 u^2 \psi(u) + \int_{-\infty}^{\infty} U(u-v)\psi(v) dv = E\psi(u). \tag{8}$$

Therefore, a transition was made from differential Eq. (3) for eigenfunctions (wave functions in the coordinate domain) and eigenvalues (corresponding to discrete energy levels) to integral (8). In this equation, the integral can be replaced by a sum, and continuous variables can be replaced by discrete ones. As a result of such transformations, the following expression is obtained:

$$4\pi^2 (s\Delta)^2 \psi(s\Delta) + \sum_{p=-\frac{(N-1)}{2}}^{\frac{(N-1)}{2}} U(s\Delta - p\Delta)\psi(p\Delta)\Delta = E\psi(s\Delta), \tag{9}$$

where $\Delta = u_{\max} / N$, $u_s = s\Delta$, $v_p = p\Delta$, $-(N-1)/2 \le s, p \le (N-1)/2$, s, p and N are integers. $u_{\max}$ should be taken so that at frequencies $|u| \ge u_{\max}/2$ the values $\psi(u)$ are almost equal to zero. The value of N must be large and preferably unpaired. Obviously, the sum in Eq. (9) should have N elements.

The last equation can be written for all discrete spatial frequencies $u_s = s\Delta$, where s changes between $-(N-1)/2$, and $(N-1)/2$, then a set of equations in the amount of N can be written in a matrix form, where E is common for all values of s:

$$(\mathbf{P} + \mathbf{U})\Psi = E\Psi, \tag{10}$$

where P is a diagonal matrix with elements $4(\pi s\Delta)^2$, U is a square symmetric matrix with elements $U(s\Delta - k\Delta)$, Ψ is a vector-column with elements $\psi(s\Delta)$.

Therefore, in (10), Ψ is a discrete Fourier transform of a wave function that corresponds to a discrete energy level E and must be valid according to the postulates of

quantum mechanics. In the case of several eigenvalues and corresponding eigenvectors, the eigenfunction $\psi(x)$ was obtained after the inverse discrete Fourier transform of the eigenvector.

To search for discrete energy levels of electrons and holes in quantum wells, the structure shown in Fig. 1b is "split" into three substructures: the zero level of potential energy will be at -4 eV for electrons and -5.9 eV for holes, respectively; the band gap will be 1.9 eV.

Thus, in the quantum structure for electrons, there will be the following changes in the energy limits for the corresponding layers (from left to right): $-2.1 \to 1.9, -2 \to 2,$ $-2.4 \to 1.6, -4.0 \to 0, -2.5 \to 1.5, -4.0 \to 0, -2.5 \to 1.5, -4.0 \to 0, -2.5 \to 1.5,$ $-2.7 \to 1.3$; similar changes for holes will be as follows: $-5.2 \to 0.7, -5.5 \to 0.4, -6.0 \to -0.1, -5.9 \to 0, -6.8 \to -0.9,$ $-5.9 \to 0, -6.8 \to -0.9, -5.9 \to 0, -6.8 \to -0.9,$ $-6.0 \to -0.1$.

Since the main task is to find wave functions and the corresponding energy levels of electrons and holes localized in quantum wells, it is necessary to set the upper energy limit for electrons at the level of $-2.7 - (-4) = 1.3\text{eV}$, the corresponding limit for holes is $-6 - (5.9) = -0.1\text{eV}$

Due to the effective electron mass $m_e^* = 11.3m_0$, the discrete energy levels number will get 114 for electrons. The three lowest energy levels are 0.00128334 eV, 0.00128335eV, and 0.00128414 eV. They are adjacent to the bottom of the quantum well. Fig. 5 shows the moduli of wave functions superimposed on the energy diagram for electrons. It should be noted that the energy diagram is enlarged along the ordinate axis by 10^4. So, 1.5 eV corresponds to 15 thousand conventional units. The wave functions calculated by the method described above are orthonormal, and the numerically calculated deviation from orthonormality is less than 10^{-9}, which indicates the high accuracy of the calculation by the proposed method.

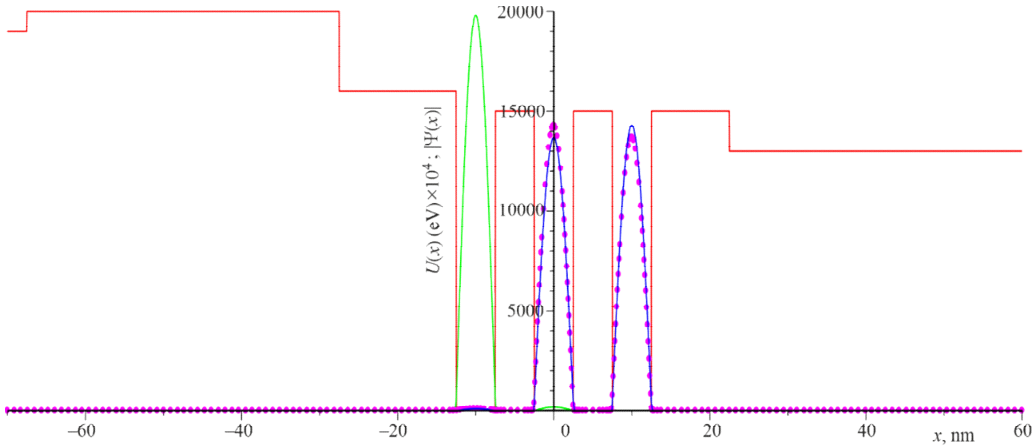

Fig. 5. Energy diagram for electrons (red), moduli of wave functions corresponding to energy levels: E_{11}=0.00128334 eV (blue), E_{12}=0.00128335 eV (magenta, dot), E_{13}=0.00128414 eV (green).

The values of E_{11} and E_{12} differ slightly; the magnitudes of the corresponding wave functions also show minor differences. However, these functions are orthogonal, and their real and imaginary parts are distinct. Fig. 6 shows the modules of three wave functions for the following three corresponding energy levels: 0.0051334 eV, and 0.0051367 eV. Each of these wave functions crosses zero only once within the quantum wells.

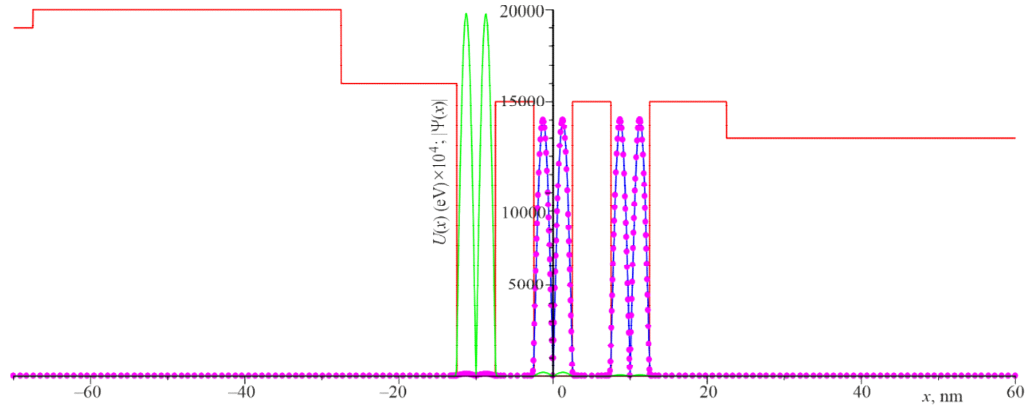

Fig. 6. Energy diagram for electrons (red), moduli of wave functions corresponding to energy levels: E_{21}=0.0051334 eV (blue), E_{22}=0.0051335 eV (magenta, dot), E_{23}=0.0051367 eV (green).

It should be noted that the ratio $E_{2,j} / E_{1,j}$ is approximately equal to 4, which holds for two series of energy levels in rectangular wells of finite height. Each series has three closely spaced levels, as the three quantum wells share the same width. The three energy levels in the next series are E_{31}=0.015496 eV, E_{32}=0.015497 eV, and E_{33}=0.015569 eV. The corresponding wave functions in each quantum well intersect the x-axis twice.

Calculations of the energy levels and corresponding wave functions for holes with a mass of $m_h^* = -2.26 m_0$ were also performed. A total of 20 energy levels for holes were obtained, which is fewer than the number of levels for electrons since the effective mass of holes is significantly smaller than the electron mass. In addition, the energy constraint by modulus for holes is 0.1 eV, which is lower than the corresponding constraint for electrons (1.3 eV). The three highest energy levels are as follows: -0.00539945 eV, -0.00598265 eV, and -0.00598266 eV. The calculation results of the moduli of the corresponding wave functions are presented in Fig. 7.

Fig. 8 shows the moduli of the wave functions corresponding to the following three energy levels: -0.021497 eV. -0.0239223 eV, and -0.0239224 eV. Each of the subsequent

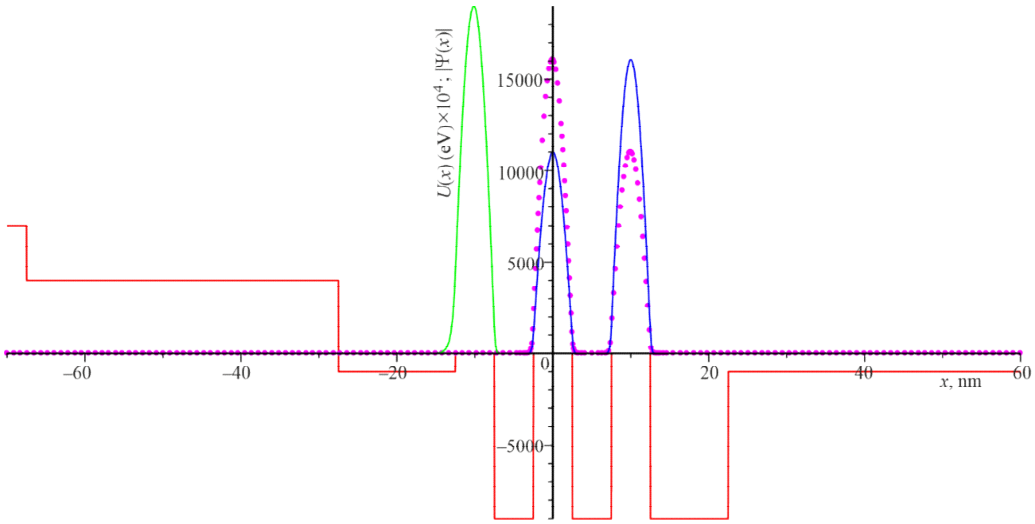

Fig. 7. Energy diagram for holes (red), moduli of wave functions corresponding to energy levels: E_{11}=-0.00539945 eV (green), E_{12}=-0.00598265 eV (magenta, dot), E_{13}=-0.00598266 eV (blue).

three wave functions in each quantum well crosses zero once. The calculation results also indicate that two energy levels are extremely close, differing at the seventh or eighth decimal place, for instance, -0.0239223 eV and -0.0239224 eV. This slight difference in energy levels may suggest level degeneracy; however, the corresponding wave functions are distinct, which is consistent with the principles of quantum mechanics.

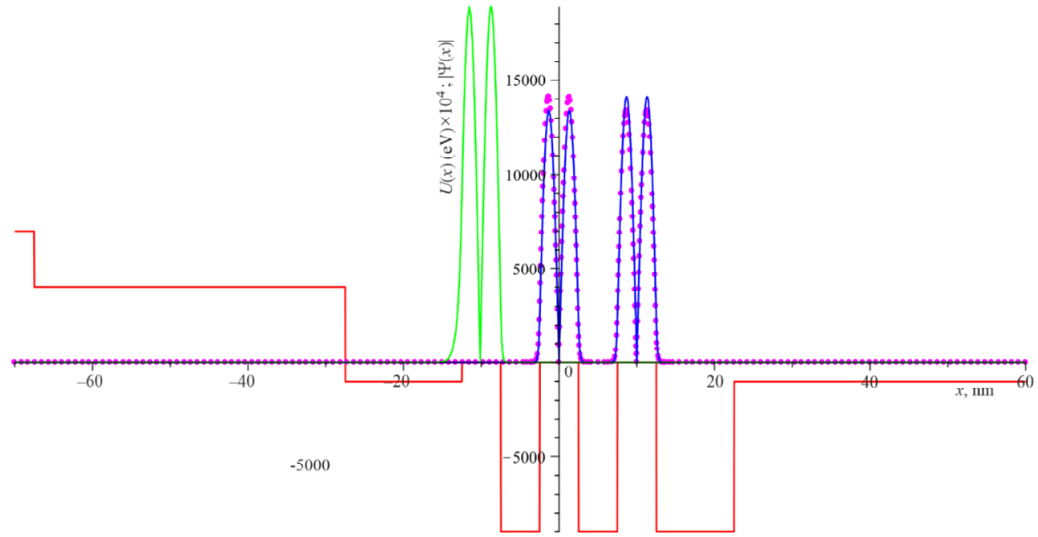

Fig. 8. Energy diagram for holes (red), moduli of wave functions corresponding to energy levels: E_{21}=-0.021497 eV (green), E_{22}=-0.0239223 eV (magenta, dot), E_{23}=-0.0239224 eV (blue).

Therefore, for certain discrete electron and hole levels, strong carrier localization is observed in the quantum wells, which corresponds to a significant increase in the modulus of the wave functions within these wells. Since the effective masses of electrons and holes are substantially larger than the free electron mass, and the quantum well width is sufficiently large (5 nm), the discrete energy levels near the conduction band minimum and valence band maximum are significantly lower than 1 eV. To increase the energy of the discrete levels, it is necessary to reduce the width of the quantum wells and decrease the effective mass of the charge carriers.

4. Conclusions

To summarize, an OLED with quantum wells structure using 4CzTPN-Ph as the emitter was fabricated, and its electroluminescent properties were studied in detail, comparing with a doped OLED based on the same emitter. The optimized electroluminescent device with a TSPO1 layer as a potential well exhibits a maximum brightness of 420 cd/cm^2 and a peak current efficiency of 1.8 cd/A. Furthermore, the quantum efficiency roll-off was significantly reduced. The device also exhibited a narrow electroluminescence spectrum close to the coordinates of spectrally pure red color. The proposed concept of forming quantum wells in OLED technology will be useful for the further design of OLEDs with MQW structure, aimed at simplifying the manufacturing process and increasing device efficiency. The solution of the one-dimensional stationary Schrödinger equation for a multilayer light-emitting structure showed that electrons and holes in quantum wells are localized. The significant magnitude of the wave function moduli in quantum wells confirms the localization of charge carriers. Since there are three quantum wells in the studied structure, a corresponding splitting of energy

levels is observed, which are close to each other, and each of them has its wave function, which is orthogonal. The effective electron and hole masses were determined through the analysis of the band structure of the 4CzTPN-Ph crystal. The results indicate that the effective mass for electrons is higher than that for holes, which can be attributed to the smaller curvature of the CBM compared to the VBM. Consequently, the molecular structure of 4CzTPN-Ph, comprising multiple carbazole units, facilitates higher hole mobility than electron mobility, making this material particularly well-suited for OLED applications.

Acknowledgement. The research presented in this paper was funded by the European Union under Horizon Europe for the HELIOS project (Grant Agreement 101155017). This project has also received funding from the Research Council of Lithuania, project QUANT (Grant Agreement No S-LU-24-8), and the National Science Foundation (NSF) (Grant No OAC-2118091) in the framework of the Scientific Cooperation Program between Lithuania and Ukraine. The DFT work used the Expanse cluster at SDSC through allocation PHY180014 from the Advanced Cyberinfrastructure Coordination Ecosystem: Services & Support (ACCESS) program, which is supported by National Science Foundation Grants No 2138296.

References

1. Zhang, D., Duan, L., Zhang, Y., Cai, M., Zhang, D., & Qiu, Y. (2015). Highly efficient hybrid warm white organic light-emitting diodes using a blue thermally activated delayed fluorescence emitter: exploiting the external heavy-atom effect. *Light: Science & Applications*, *4*(1), e232.
2. Li, C., Duan, R., Liang, B., Han, G., Wang, S., Ye, K., Liu, Y., Yi, Y., & Wang, Y. (2017). Deep-Red to Near-Infrared Thermally Activated Delayed Fluorescence in Organic Solid Films and Electroluminescent Devices. *Angewandte Chemie International Edition*, *56*(38), 11525–11529.
3. Liu, C., Li, J., Man, X., Liu, H., Sun, X., Liu, F., & Lu, P. (2018). Synthesis and Characteristics of New Organic Red Emissive Materials Based on Phenanthro[9,10- d]imidazole. *Chemistry – An Asian Journal*, *14*(6), 821–827.
4. Hu, Y., Yuan, Y., Shi, Y.-L., Li, D., Jiang, Z.-Q., & Liao, L.-S. (2018). Efficient Near-Infrared Emission by Adjusting the Guest-Host Interactions in Thermally Activated Delayed Fluorescence Organic Light-Emitting Diodes. *Advanced Functional Materials*, *28*(32), 1802597.
5. Wang, H., Xie, L., Peng, Q., Meng, L., Wang, Y., Yi, Y., & Wang, P. (2014). Novel Thermally Activated Delayed Fluorescence Materials-Thioxanthone Derivatives and Their Applications for Highly Efficient OLEDs. *Advanced Materials*, *26*(30), 5198–5204.
6. Sun, Y., Sun, W., Liu, W., Li, X., Yin, J., & Zhou, L. (2022). Efficient Nondoped Pure Red/Near-Infrared TADF OLEDs by Designing and Adjusting Double Quantum Wells Structure. *ACS Applied Electronic Materials*, *4* (7), 3615-3622.
7. Zhang, Q., Li, B., Huang, S., Nomura, H., Tanaka, H., & Adachi, C. (2014). Efficient blue organic light-emitting diodes employing thermally activated delayed fluorescence. *Nature Photonics, 8*(4), 326–332.
8. Shimizu, M., Kaki, R., Takeda, Y., Hiyama, T., Nagai, N., Yamagishi, H., & Furutani, H. (2012). 1,4-Bis(diarylamino)-2,5-bis(4-cyanophenylethenyl)benzenes: Fluorophores Exhibiting Efficient Red and Near-Infrared Emissions in Solid State. *Angewandte Chemie, 124*(17), 4171–4175.
9. Caspar, J. V., Kober, E. M., Sullivan, B. P., & Meyer, T. J. (1982). Application of the energy gap law to the decay of charge-transfer excited states. *Journal of the American Chemical Society, 104*(2), 630–632.
10. Chen, J.-X., Wang, K., Zheng, C.-J., Zhang, M., Shi, Y.-Z., Tao, S.-L., Ou, X.-M., Zhang, X.-H. (2018). Red organic light-emitting diode with external quantum efficiency beyond 20% based on a novel thermally activated delayed fluorescence emitter. *Advanced Science*, 1800436.
11. Hladka, I., Lytvyn, R., Volyniuk, D., Gudeika, D., & Grazulevicius, J. V. (2018). W-shaped bipolar derivatives of carbazole and oxadiazole with high triplet energies for electroluminescent devices. *Dyes and Pigments, 149,* 812–821.
12. Danyliv, Y., Volyniuk, D., Bezvikonnyi, O., Hladka, I., Ivaniuk, K., Helzhynskyy, I., Stakhira, P., Tomkeviciene, A., Skhirtladze, L., Grazulevicius, J. V. (2019). Through-space charge transfer in luminophore based on phenyl-linked carbazole- and phthalimide moieties utilized in cyan-emitting OLEDs. *Dyes and Pigments*, 107833.
13. Yingkui, L. (2011). Nondoped phosphorescent organic quantum well light-emitting device based on iridium complex: Synthesis, characterization, photophysical property, and electroluminescence performance. *Journal of Luminescence, 131*(9), 1821–1826.

14. Miller, D. A. B. (2020). Optical physics of quantum wells, in Quantum Dynamics of Simple Systems. *CRC Press, Boca Raton*, 239–266.
15. Uoyama, H., Goushi, K., Shizu, K., Nomura, H., & Adachi, C. (2012). Highly efficient organic light-emitting diodes from delayed fluorescence. *Nature*, *492*(7428), 234–238.
16. Deng, J., Jia, W., Chen, Y., Liu, D., Hu, Y., & Xiong, Z. (2017). Guest concentration, bias current and temperature-dependent sign inversion of magneto-electroluminescence in thermally activated delayed fluorescence devices. *Scientific Reports, 7*(1), 44396.
17. Giannozzi, P. et al., (2009) Quantum espresso: a modular and open-source software project for quantum simulations of materials. *J. Phys.: Condens. Matter.*, *21*(39), 395502.
18. Perdew, J. P.; Burke, K.; & Ernzerhof, M. (1996) Generalized gradient approximation made simple. *Phys. Rev. Lett.* 77, 3865–3868.
19. Grimme, S.; Antony, J.; Ehrlich, S.; & Krieg, S. (2010) A consistent and accurate *ab initio* parametrization of density functional dispersion correction (DFT-D) for the 94 elements H-Pu. *J. Chem. Phys.*, *132*, 154104.
20. Stakhira, P., Cherpak, V., Volynyuk, D., Ivastchyshyn, F., Hotra, Z., Tataryn, V., & Luka, G. (2010). Characteristics of organic light emitting diodes with copper iodide as injection layer. *Thin Solid Films, 518*(23), 7016–7018.
21. Kim, B. S., & Lee, J. Y. (2014). Engineering of Mixed Host for High External Quantum Efficiency above 25% in Green Thermally Activated Delayed Fluorescence Device. *Advanced Functional Materials, 24*(25), 3970–3977.
22. Sun, D., Ren, Z., Bryce, M. R., & Yan, S. (2015). Arylsilanes and siloxanes as optoelectronic materials for organic light-emitting diodes (OLEDs). *Journal of Materials Chemistry C, 3*(37), 9496–9508.
23. Hatakeyama, T., Shiren, K., Nakajima, K., Nomura, S., Nakatsuka, S., Kinoshita, K., Ni, J., Ono, Y., Ikuta, T. (2016). Ultrapure blue thermally activated delayed fluorescence molecules: efficient HOMO-LUMO separation by the multiple resonance effect. *Advanced Materials, 28*(14), 2777–2781.
24. Lee, C. W., & Lee, J. Y. (2013). Above 30% external quantum efficiency in blue phosphorescent organic light-emitting diodes using Pyrido[2,3-b]indole derivatives as host materials. *Advanced Materials, 25*(38), 5450–5454.
25. Tsiko, U., Volyniuk, D., Andruleviciene, V., Leitonas, K., Sych, G., Bezvikonnyi, O., Jasinskas, V., Gulbinas, V., Stakhira, P. & Grazulevicius, J. V. (2022). Triphenylamino or 9-phenyl carbazolyl-substituted pyrimidine-5-carbonitriles as bipolar emitters and hosts with triplet harvesting abilities. *Materials Today Chemistry,* 25, 100955.
26. Huh, J.-S., Kim, K.-H., & Kim, J.-J. (2020). Emitting dipole orientation and molecular orientation of homoleptic Ir(III) complexes. *Organic Electronics, 82,* 105715.
27. Wang, J., Yu, J., Li, L., Wang, T., Yuan, K., & Jiang, Y. (2008). Low roll-off power efficiency organic light-emitting diodes consisted of nondoped ultrathin phosphorescent layer. *Applied Physics Letters, 92*(13), 133308.
28. Liu, S. M., Li, B., Zhang, L. M., & Yue, S. M. (2011). Low-Voltage, High efficiency nondoped phosphorescent organic light-emitting devices with double-quantum-well structure. *Applied Physics Letters*, *98*, 163301.
29. Wex, B., & Kaafarani, B. R. (2017) Perspective on carbazole-based organic compounds as emitters and hosts in TADF applications. J. Mater. Chem. C, *5*, 8622–8653.
30. Liu, Z., Lei, Y., Fan, C., Peng, X., Ji, X., Jabbour, G.E., & Yang, X. (2017) Simple-structure organic light emitting diodes: Exploring the use of thermally activated delayed fluorescence host and guest materials. Org. Electron., *41*, 237–244.
31. Nishide, J., Nakanotani, H., Hiraga, Y., & Adachi, C. (2014) High-efficiency white organic light-emitting diodes using thermally activated delayed fluorescence. *Appl. Phys. Lett.*, *104*, 233304.
32. Fitio, V. M., Yaremchuk, I. Y., Romakh, V. V., & Bobitski, Y. V. (2015). A solution of one-dimensional stationary Schrodinger equation by the Fourier transform. *ACES Journal*, *30*(5), 534-539.
33. Goodman, J. W. (1968). *Introduction to Fourier Optics*. McGraw-Hill Companies, Inc.

L. Deva, P. Stakhira, V. Fitio, S. Debata, P. Dev, N. Karaush-Karmazin, N. Kuzyk, I. Yaremchuk, D. Volyniuk. (2025). Organic Light-Emitting Devices with Quantum Well Structures Using Carbazole Derivative 4CzTPN-Ph as an Emitting Material**.** *Ukrainian Journal of Physical Optics*, *26*(1), 01009 – 01022. doi: 10.3116/16091833/Ukr.J.Phys.Opt.2025.01009

Анотація. *В роботі досліджені електролюмінісцентні властивості органічних світловипромінювальних діодів (OLED) на основі похідної карбазолу (4CzTPN-Ph), якій притаманне випромінювання червоного кольору. З цією метою, на основі цього емітера, було сформовано два типи OLED: перший — на основі системи «гість-господар», другий – світловипромінююча структура з потрійним каскадом квантових ям.*

У другому OLED ультратонкий емітер 4CzTPN-Ph (товщина шару 5 нм) був розміщений між шарами mCBP і TSPO1 для першої ями, а також між однотипними шарами TSPO1 для другої та третьої квантових ям. Така конфігурація дала змогу сформувати оптимальні енергетичні бар'єри на інтерфейсах для розсіювання носіїв та екситонів у кожній ямі, а також сприяла розширенню зони рекомбінації носіїв та зменшенню ймовірності гасіння екситонів. Розрахунок дискретних рівнів електронів і дірок у квантових ямах проводився шляхом розв'язку стаціонарного рівняння Шредінґера. Розрахунки показали локалізацію електронів і дірок у відповідних квантових ямах. Комплексний порівняльний аналіз ефективності OLED-пристроїв (яскравості, енергоефективності, струмової ефективності) показав, що в першому типі OLED, завдяки відносно широкому спектральному перекриттю випромінювання компоненти господаря (mCBP) зі спектром поглинання емітера 4CzTPN-Ph, відбувається ефективна передача енергії до емітера. Як наслідок, OLED з системою «гість–господар» демонструє зовнішню квантову ефективність на рівні 2% при максимальній яскравості понад 1000 кд/м². Загалом свіловипромінюючий пристрій другого типу володіє дещо гіршими параметрами, проте перевагою OLED з каскадом квантових ям, завдяки наявності вузької ширини квантових ям (5 нм), є характерне звуження спектру електролюмінесценції та координати спектрально чистішого червоного кольору CIE (0.58, 0.33) відносно спектру легованого OLED з координатами CIE (0.51, 0.38). Таким чином вирішена проблема зсуву спектра червоного випромінювання в синю область, що притаманна OLED структурам з системою «гість-господар».

Ключові слова: *OLED, квантова яма, екситон, гетероструктура, система «гість-господар»*